

Diff-Palm: Realistic Palmprint Generation with Polynomial Creases and Intra-Class Variation Controllable Diffusion Models

Jianlong Jin^{1*}, Chenglong Zhao^{2*}, Ruixin Zhang², Sheng Shang¹, Jianqing Xu², Jingyun Zhang³, ShaoMing Wang³, Yang Zhao¹, Shouhong Ding^{2†}, Wei Jia^{1†}, Yunsheng Wu²

¹ Hefei University of Technology, ² Tencent Youtu Lab, ³ Tencent WeChat Pay Lab33

jianlong@mail.hfut.edu.cn, lornezhao@tencent.com

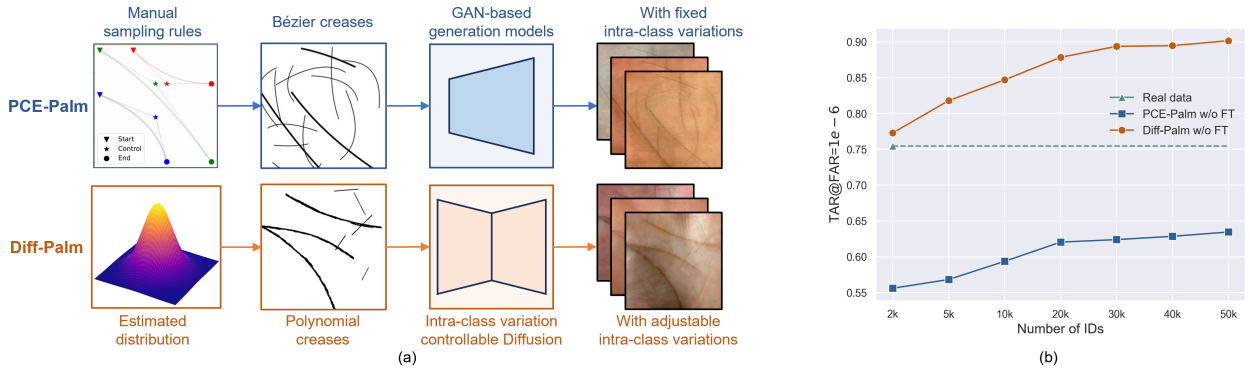


Figure 1. Comparison between PCE-Palm [22] and the proposed Diff-Palm. (a) PCE-Palm adopts conditional GAN with Bézier creases [48] as input to generate palmprint datasets. Diff-Palm introduces a polynomial crease and a novel diffusion model for synthesizing datasets with adjustable intra-class variations. (b) The average performance of recognition models, trained on three types of datasets (real data, PCE-Palm generated, and Diff-Palm generated) and evaluated on five public datasets. (FT: Fine-tune) Code: <https://github.com/Ukuer/Diff-Palm>

Abstract

Palmprint recognition is significantly limited by the lack of large-scale publicly available datasets. Previous methods have adopted Bézier curves to simulate the palm creases, which then serve as input for conditional GANs to generate realistic palmprints. However, without employing real data fine-tuning, the performance of the recognition model trained on these synthetic datasets would drastically decline, indicating a large gap between generated and real palmprints. This is primarily due to the utilization of an inaccurate palm crease representation and challenges in balancing intra-class variation with identity consistency. To address this, we introduce a polynomial-based palm crease representation that provides a new palm crease generation mechanism more closely aligned with the real distribution. We also propose the palm creases conditioned diffusion model with a novel intra-class variation control method. By applying our proposed K -step noise-sharing sampling, we are able to synthesize palmprint datasets with large intra-class variation and high identity consistency. Experiments

show that, for the first time, recognition models trained solely on our synthetic datasets, without any fine-tuning, outperform those trained on real datasets. Furthermore, our approach achieves superior recognition performance as the number of generated identities increases.

1. Introduction

Palmprint recognition has gained widespread interest for its highly discriminative, user-friendly, and privacy-friendly nature [13]. However, its further development is severely limited by the lack of large-scale public datasets. With the remarkable results achieved by deep generative models, such as Generative Adversarial Networks (GANs) [17] and Diffusion models [20], generating datasets for recognition tasks is a promising and valuable approach to replace the collection of large-scale real datasets [23].

Although existing palmprint generation methods, including RPG-Palm [36] and PCE-Palm [22] have obtained impressive results, they still rely on fine-tuning with real data to obtain good recognition performance. Specifically, they generate large-scale data to pre-train the recognition mod-

*Equal contribution. † Corresponding authors.

els and then fine-tune them with real data. However, without fine-tuning, the recognition model’s performance suffers from significant degradation, indicating a large gap between the generated data and real data.

We have identified two principal factors contributing to the observed issue. The first factor is the **inaccurate representation of palm creases**. Existing methods [22, 36] employ manually designed Bézier curves [48] to simulate palm creases. However, these curves significantly differ from the actual patterns found in genuine palmprints, resulting in a substantial divergence between synthetic and real palmprint data. Furthermore, the use of merely three control points per Bézier curve restricts its expressiveness. The second factor is the **challenges in balancing intra-class variation with identity consistency**. In the context of palmprint image generation, these methods [22, 36] employ conditional GANs and simulate intra-class variations of palmprints by adding a simple random noise. This strategy, however, yields datasets with large intra-class variation and low identity consistency compared to real datasets, thereby leading to diminished performance.

To address the aforementioned issues, we propose a novel framework to generate realistic palmprint datasets with large intra-class variation and high identity consistency, which achieves superior performance compared to the existing SOTA method, i.e., PCE-Palm [22], as shown in Fig. 1. Specifically, we utilize polynomial curves to describe palm creases, termed polynomial creases. To achieve a more accurate and expressive representation, we employ fourth-order polynomial curves parameterized by five coefficients, which substantially expands the sampling space. Based on the statistical analysis of real palm creases, we estimate a multivariate Gaussian distribution for the coefficients of polynomial curves. Subsequently, we develop a new sampling mechanism that obtains coefficients from the estimated Gaussian distribution to synthesize polynomial palm creases. This approach effectively reduces the discrepancy between synthetic and real palm creases.

Furthermore, we introduce a novel intra-class variation controllable diffusion model, designed to generate palmprints datasets that exhibit substantial variation while preserving high identity consistency. Diffusion models [20] synthesize images via a denoising sampling process. However, the inherent randomness of this process typically results in uncontrollable variation within the same identity class, potentially compromising identity consistency. This issue can lead to generated datasets with excessive intra-class variation and diminished identity consistency. To tackle this problem, we propose a simple yet effective sampling method, termed K -step noise-sharing sampling. This method enhances the diffusion model by employing shared noise across samples within the same identity during the sampling process, instead of distinct noise sequences. By

adjusting the parameter K , we are able to generate datasets with a spectrum of intra-class variations. Notably, the proposed K -step noise-sharing sampling can be used as a plug-and-play module applied in other diffusion models.

In our experimental setup, we train recognition models with synthetic datasets, and evaluate them directly on publicly available datasets without employing any real data fine-tuning. Our contributions are as follows:

- We introduce a more realistic palm crease representation based on polynomial curves, which not only exhibits high expressive capability but also ensures that generated palm creases align with the distribution of real ones.
- We propose a novel intra-class variation controllable diffusion model with a K -step noise-sharing sampling. It utilizes palm creases as identity conditions, enabling the synthesis of palmprint datasets that exhibit large intra-class variation while preserving high identity consistency.
- Through extensive open-set experiments, we demonstrate for the first time that recognition models trained solely on synthetic datasets generated by our method outperform those trained on real datasets, without the benefit of real data fine-tuning. Moreover, our approach shows a significant improvement in performance as the number of generated identities increases.

2. Related Work

2.1. Data Generation for Biometric Recognition

With advancements in generation methods [3], various models have been employed to create synthetic samples in the field of biometrics, such as face generation [8, 14, 15, 24, 31, 32, 41], and fingerprint synthesis [1, 11, 37]. For palmprint generation, Bézierpalm [48] firstly utilizes Bézier curves to represent palm creases and generates new identities by sampling random curves. Subsequently, both RPG-Palm [36] and PCE-Palm [22] employ Bézier curves as an identity condition and GAN-based generative models for palmprint generation. Although these methods can produce visually realistic palmprint images, they still need to be fine-tuned with real data to achieve satisfactory results.

2.2. Conditional Diffusion Models

Diffusion models have achieved remarkable performance in numerous visual tasks [5, 49]. To enable controllable generation, two main conditional control mechanisms are employed. The first is the embedding-based conditional approach [25, 33], where the embedding is typically derived from the output of a pre-trained model. This extracted embedding is then incorporated into the UNet network architecture through a cross-attention mechanism. The second is the channel-based conditional approach [30, 34], where conditional images are concatenated with the diffused image through channels. For our research, we utilize

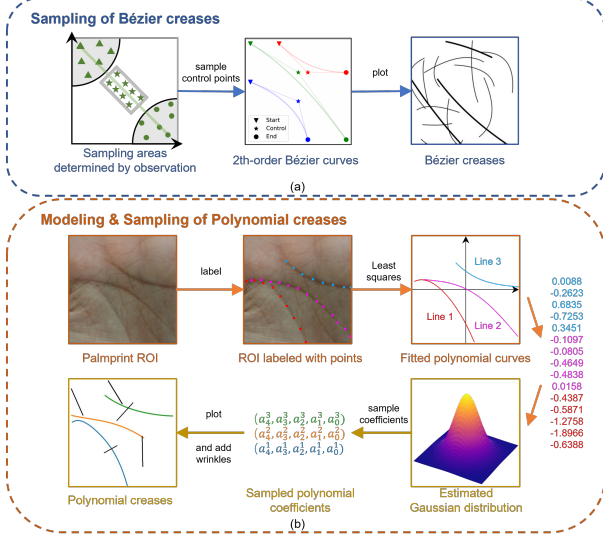


Figure 2. Comparison of (a) Bézier creases [48] and (b) proposed polynomial creases.

the channel-based conditional diffusion model as our baseline, as it ensures a strong correspondence between conditional images and generated images. Furthermore, we draw comparisons with the embedding-based conditional model, IDiff-Face [2], an identity-conditioned face generation method with impressive recognition performance.

2.3. Recognition Methods

Deep learning has significantly advanced biometric recognition, especially in facial recognition, where margin-based methods like CosFace [39] and ArcFace [7] have shown exceptional performance. Similarly, in palmprint recognition, several deep learning methods have been proposed [12, 16, 21, 42, 43, 50], many of which introduce refined networks accompanied by margin-based loss. Thus, this paper adopts ArcFace as the palmprint recognition baseline to compare different generation methods, as in PCE-Palm [22].

3. Methods

In this section, we first introduce a polynomial representation for palm creases, which synthesize pseudo palm creases as identity conditions for generating realistic palmprints. We then propose an intra-class variation controllable diffusion model, which includes palm creases conditioned diffusion and a K -step noise-sharing sampling mechanism. Utilizing these components, we are able to generate palmprint datasets with adjustable levels of intra-class variations.

3.1. Polynomial Representation for Palm Creases

Current palmprint generation models [22, 36] rely on palm creases as identity control conditions, making palm crease representation a crucial task for palmprint genera-

tion. These models all employ second-order Bézier curves to represent palm creases [48], as follows,

$$\mathbf{B}(t) = (1-t)^2\mathbf{P}_s + 2t(1-t)\mathbf{P}_c + t^2\mathbf{P}_e, \quad (1)$$

where $\mathbf{P}_s, \mathbf{P}_c, \mathbf{P}_e$ represent starting point, control point, and ending point respectively, which are randomly sampled within a predefined artificial area range, and t is the parameter ranging from 0 to 1, determining the position along the curve, as shown in Fig.2 (a). However, although existing generation-based methods [22, 36] can produce visually realistic palmprint images, the distribution of simulated palm creases is quite different from that of real palm creases, leading to the requirement of fine-tuning on real data.

To overcome this limitation, this paper focuses on enhancing palm crease representation to align more closely with the distribution of real palm creases. Consequently, we propose a polynomial representation for palm creases, and derive the estimated distribution of the representation parameters through statistical analysis. The proposed polynomial representation is defined as follows,

$$y^i = a_4^i x^4 + a_3^i x^3 + a_2^i x^2 + a_1^i x + a_0, \quad (2)$$

where $[a_4^i, a_3^i, a_2^i, a_1^i, a_0^i]$ denote polynomial coefficients, and $i(i = 1, 2, 3)$ represents three principal lines of the palmprint. Compared to the second-order Bézier curves, a fourth-order polynomial representation provides sufficient expressiveness to capture the smoothness of palm creases. Additionally, considering the physiological basis and distinct distribution of palm creases, it is essential to sample curve parameters that reflect the actual distribution.

As shown in Fig.2 (b), we manually label the points on the three principal lines of 1000 palmprint ROI images selected from publicly available datasets. For each line, the polynomial coefficients are calculated using the least squares method, based on n labeled points $((x_0, y_0), (x_1, y_1), \dots, (x_{n-1}, y_{n-1}))$, as follows,

$$\mathbf{a}^T = (\mathbf{X}^T \mathbf{X})^{-1} \mathbf{X}^T \mathbf{y}, \quad (3)$$

where \mathbf{a}^T represents coefficient vector $[a_0, a_1, \dots, a_4]^T$, \mathbf{y} represents vector $[y_0, y_1, \dots, y_{n-1}]^T$, and $\mathbf{X} \in \mathbb{R}^{n \times 5}$ is a Vandermonde matrix. We apply this formula to get coefficient vectors $(\mathbf{a}^1, \mathbf{a}^2, \mathbf{a}^3)$ of three principal lines.

In this way, polynomial coefficients of three principal lines $(\mathbf{a}^1, \mathbf{a}^2, \mathbf{a}^3)$ are calculated for each palmprint sample. Then, we conduct a statistical analysis of the polynomial coefficients. Partial visualization results are shown in Fig.3, from which we observe that the coefficient approximately follows a Gaussian distribution. More statistical results are provided in the supplementary materials. Consequently, we represent the distribution of a_j^i as $p(a_j^i) \sim N(\mu_j^i, (\sigma^2)_j^i)$, where μ_j^i and $(\sigma^2)_j^i$ denote mean and variance of a_j^i . Therefore, the coefficient vector \mathbf{a}^i follows the joint distribution

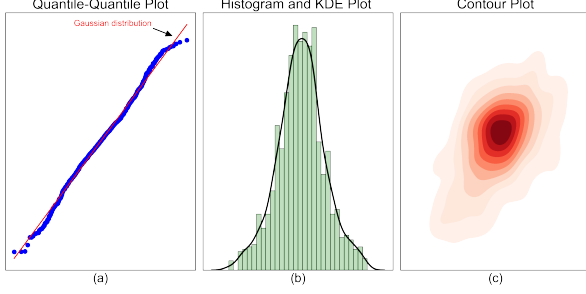


Figure 3. Statistical analysis of polynomial coefficients: (a) Quantile-Quantile Plot of coefficients a_4^1 . (b) Histogram and Kernel Density Estimate (KDE) Plot of coefficients a_4^1 . (c) Contour Plot of coefficients a_4^1 and a_3^1 .

$p(a_0^i, a_1^i, \dots, a_4^i)$, which is a multivariate Gaussian distribution expressed as follows,

$$p(\mathbf{a}^i) \sim \mathcal{N}(\mu^i, \Sigma^i), \quad (4)$$

where μ^i, Σ^i are the mean vector and covariance matrix of \mathbf{a}^i . By employing the proposed representation and estimated distribution, the complex palm creases located on a plane are mapped into a parameter space that conforms to a multivariate Gaussian distribution. This allows us to effortlessly sample the polynomial coefficients from the statistical distribution and then produce three principal lines using polynomial representation.

Additionally, we also record the coordinates of two endpoints of each line, i.e., the starting point x_s^i and the ending point x_e^i , and calculate their statistical distribution. By following the same approach, we determine the range for synthesizing polynomial creases by sampling from the estimated distribution. With the addition of minor random straight lines to simulate wrinkles, a pseudo palm crease image is generated, as shown in Fig.2.

A palm creases similarity control mechanism is proposed by scaling the variance of the estimated Gaussian distribution by a factor of γ^2 . Specifically, as \mathbf{a}^i is sampled from $\mathcal{N}(\mu^i, \gamma^2 \Sigma^i)$, a smaller γ (less than 1) results in a higher degree of similarity in the generated palm creases, while a larger γ (greater than 1) leads to lower similarity.

3.2. Palm Creases conditioned Diffusion Model

Diffusion models [5] are trained to recover an image from random noise. In contrast to GANs, which consist of two networks and utilize an adversarial loss, diffusion models adopt two processes: the diffusion process and the denoising process. The diffusion process is typically defined as a Markov chain composed of several diffusion steps. At each step, the model introduces a small amount of Gaussian noise with varying variances into the data. After a total of T steps, the data is degraded to pure Gaussian noise. The

diffusion process [5] is expressed as,

$$p(x_t | x_{t-1}) = \mathcal{N}(x_t; \sqrt{1 - \beta_t}x_{t-1}, \beta_t I), \quad (5)$$

where x_t and x_{t-1} represent the data at diffusion step t and $t-1$ respectively, and β_t is the variance schedule determined in advance that controls the amount of noise added.

The denoising process aims to learn the reverse of the diffusion process, and recover data x_0 from Gaussian noise x_T step by step. A UNet network is trained to predict the noise at the t step and thereby restore x_{t-1} from x_t . Since we aim to use the diffusion model to generate palmprint datasets, unconditional diffusion is insufficient to meet our requirements. To control the identity of generated palmprint images, we use the palm crease image as a condition. The consistent palm crease image is extracted from the real palmprint image using a palm creases extraction module (PCEM) [22]. Then, the palm creases are adopted to govern the identity of the generated palmprints. Therefore, we choose to integrate the condition image into the UNet through channel concatenation. Specifically, paired palm crease images and corrupted palmprint images are concatenated and sent to the network, as shown in Fig.4(a). We use the following training objective [5],

$$L = E_{t, x_t, \epsilon} [\|\epsilon - \epsilon_\theta(x_t, t, y)\|_2^2], \quad (6)$$

where ϵ_θ represents the parameterized network, and y stands for palm crease image.

3.3. The K -step Noise-sharing Sampling

To generate new samples, the diffusion model follows the reverse diffusion process. Starting from random Gaussian noise, the model iteratively applies the learned denoiser to remove noise and generate final outputs. The iterative sampling process [5] is expressed as follows,

$$x_{t-1} = \frac{1}{\sqrt{\alpha_t}} \left(x_t - \frac{1 - \alpha_t}{\sqrt{1 - \alpha_t}} \epsilon_\theta(x_t, t, y) \right) + \sigma_t z_t, \quad (7)$$

where α_t is defined as $1 - \beta_t$, and $\bar{\alpha}_t := \prod_{i=0}^t \alpha_i$. The σ_t is step-dependent constants, and z_t is a random noise sampled from $\mathcal{N}(\mathbf{0}, \mathbf{I})$. After the iterative process concludes, the estimate of x_0 , derived from the final iteration, is the synthesized palmprint. To control the diversity of generated results, many diffusion-based methods adopt text prompts [5, 18]. However, palmprint images are relatively simple, comprising primarily of crease and skin components, which complicates the use of text descriptions to govern diversity. We have observed that the random noise added at each step provides the randomness of the sampling process. Therefore, by controlling the random noise added to samples within the same identity, we manipulate the intra-class variation of the generated datasets effectively.

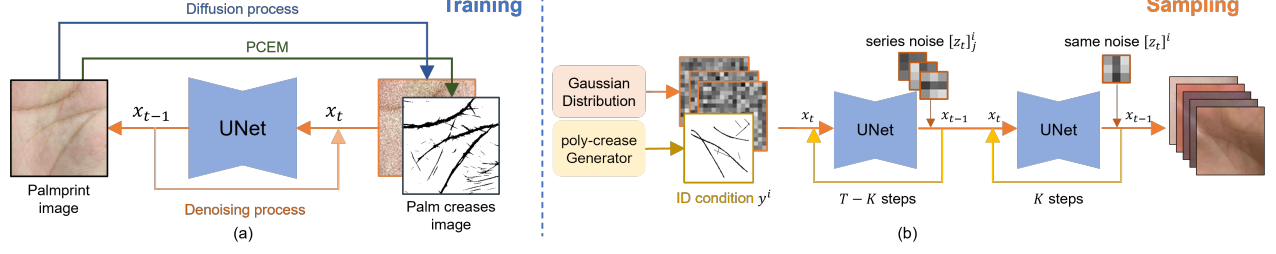


Figure 4. The proposed intra-class variation controllable diffusion model. (a) Training process: palm crease images, extracted from palmprints using PCEM [22], are employed as conditions and concatenated with diffused palmprint images, serving as input for the UNet. (b) Sampling process: polynomial creases, as synthetic identity, are first generated and adopted to create consistent samples. The K -step noise-sharing sampling is applied to obtain palmprint datasets with varying degrees of intra-class variations.

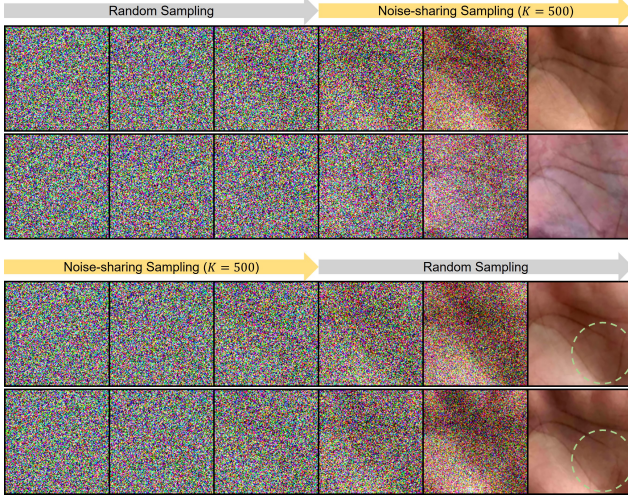


Figure 5. Generated palmprint results under different noise-sharing strategies. The figure illustrates the outcomes of applying noise-sharing in the last $K = 500$ steps (top) versus the first $K = 500$ steps (bottom) of a total $T = 1000$ steps during the sampling process for the same identity.

The K -step noise-sharing sampling is proposed to generate palmprint datasets with varying degrees of intra-class variations. Specifically, suppose generating the j -th sample of the i -th identity with the palm crease image y^i , we rewrite sampling process Eq. 7 as follows:

$$[x_{t-1}]_j^i = \frac{1}{\sqrt{\alpha_t}} \left([x_t]_j^i - \frac{1-\alpha_t}{\sqrt{1-\alpha_t}} \epsilon_\theta([x_t]_j^i, t, y^i) \right) + \sigma_t [z_t]_j^i, \quad (8)$$

where $[z_t]_j^i$ is the random noise sampled from a standard Gaussian distribution, influencing the diversity of samples. We aim to utilize the same shared noise $[z_t]_j^i$, instead of a series of different $[z_t]_j^i$ to samples under the same identity condition. We select a continuous K -step sequence within the total T steps and apply this, as shown in Fig. 4(b).

Additionally, we have found that the application of noise-sharing in the first K steps and the last K steps during the sampling process exhibits distinct behaviors. With $K = 500$ and a total of $T = 1000$ steps, the sampling

process under the same identity yields the results shown in Fig. 5. When noise-sharing is applied in the first K steps, the generated results maintain a consistent style, while the details of the palm creases exhibit minor variations, leading to a generated dataset with low identity consistency. Conversely, when noise-sharing is applied in the last K steps, the generated results present diverse styles, but the consistency of the palm crease details improves. This suggests that during the sampling process, the style information of the palmprint is generated first, followed by the restoration of texture details.

Therefore, we apply noise-sharing in the last K steps. As K increases, the crease consistency in the sampled results under the same identity tends to improve. However, when K continues to increase, the stylistic diversity of the sampled results becomes restricted. We conduct experiments on datasets generated using different values of K .

4. Experiments

4.1. Experimental Setups

We conduct experiments under an open-set protocol, splitting each public dataset into training and test sets with a 1:1 ratio with no overlapping identities (IDs). We utilize the TAR (True Accept Rate) @FAR (False Accept Rate) metric to evaluate the performance of recognition models.

Datasets We do not use public datasets to train our generative models to ensure a fair comparison, which also places our method in a more challenging cross-dataset setting. Instead, we adopt an anonymous dataset collected from the Internet, which has been processed to include 48,000 palmprint images. We utilize publicly available datasets for evaluation and to train recognition models as baselines. Experiments are conducted on following public datasets: CASIA [38], PolyU [44], Tongji [45], MPD [47], XJTU-UP [35], IITD [26], and NTU-CP-v1 [29].

Generation Model Training Setups Our conditional diffusion models utilize a UNet backbone [9] that takes a four-channel input and 64 base channels with five resolution levels. The multipliers for the number of channels used

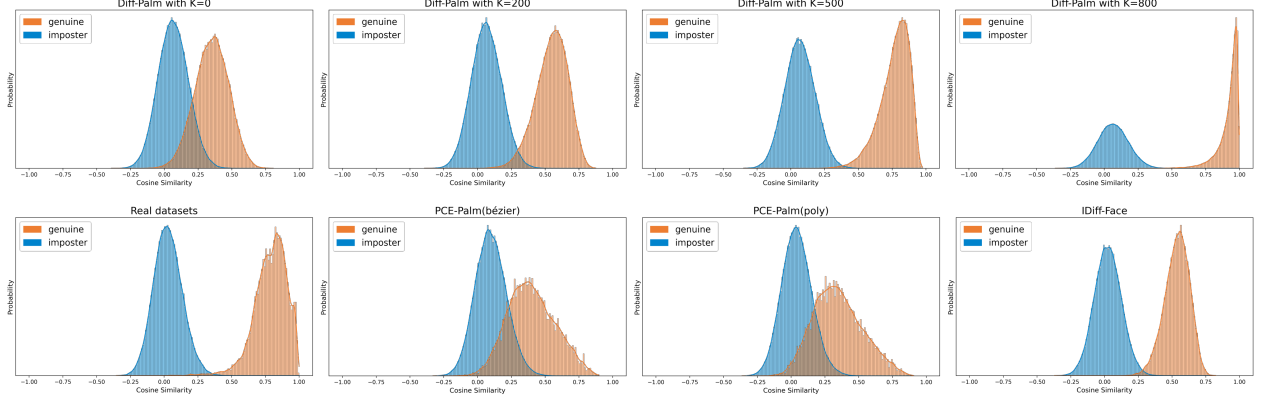


Figure 6. Comparison score plots for synthetic datasets generated by different methods and real datasets. The genuine and imposter comparison scores are calculated with features, which are extracted by a pre-trained ArcFace model from datasets.

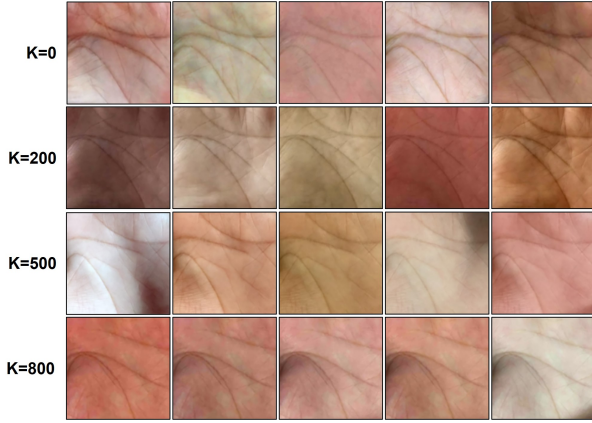


Figure 7. Example images of datasets generated by Diff-Palm with K -step sharing-noise sampling for $K = 0, 200, 500$, and 800 .

on those levels are 1, 1, 2, 3, and 4, respectively. Attention blocks are applied in residual blocks of the last resolution level. During the training process, we adopt the AdamW optimizer [27], set the learning rate $1e-4$, and train the network for a total of $30k$ steps. We apply an EMA to the weights of the model with an exponential factor of 0.9999. The batch size is 64 and is equally split across 4 GPUs. For the diffusion process, we set $T = 1000$ steps and adopt a linear diffusion variance schedule. In subsequent experiments, we default to generating datasets with $2k$ IDs and 20 samples per ID.

Recognition Model Training Setups We train ArcFace models [7] with a modified Resnet-18 [19] backbone for palmprint recognition. Palmprint images are resized to 112×112 and trained with ArcFace loss ($m = 0.5, s = 64$) over 20 epochs using a stochastic gradient descent (SGD) optimizer. We use an initial learning rate of $1e-1$, momentum of 0.9, weight decay of $5e-4$, and a step learning rate schedule, which divides the learning rate by 10 at 7-th and 15-th epoch. RandAugment [6] is adopted for data augmen-

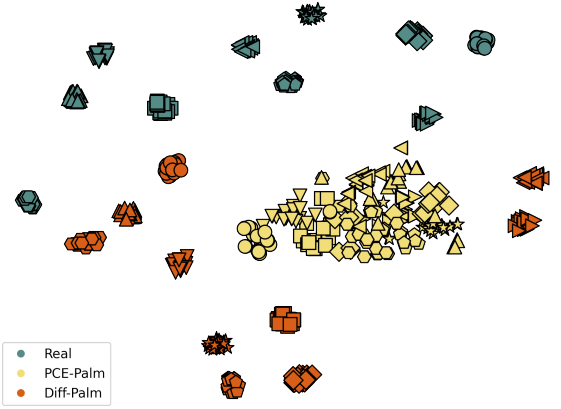


Figure 8. The t-SNE plot of features extracted from real, PCE-Palm generated, and Diff-Palm generated datasets. Colors denote different datasets, while shapes within the same color correspond to different identities.

tation with parameters (4, 4). We double the number of IDs in the training set by horizontally flipping the palmprint images. Training is implemented on 4 NVIDIA V100 GPUs with a batch size of 256. Consistent hyperparameters are used for all recognition models across various datasets.

4.2. Experimental Results

Evaluating Intra-Class Variation We generate datasets by Diff-Palm with K -step sharing-noise sampling for $K = 0, 200, 500$ and 800 . Then, we use the ArcFace model pre-trained on real datasets to extract features from synthesized datasets and calculate genuine and imposter score distributions. Comparison score plots and example images are shown in Fig.6 and Fig.7 respectively. As K increases, intra-class variation decreases, and the genuine distribution shifts right. The verification performance in Tab.1 reveals that the recognition model trained on the synthesized dataset with $K = 500$ achieves higher recognition performance.

Methods	Configs		Score Distributions				Performance (TAR@FAR=1e-6) \uparrow					
	K	γ	genuine		imposter		CASIA	PolyU	Tongji	MPD	XJTU-UP	Avg.
Diff-Palm	0	1.0	0.350	0.124	0.069	0.112	0.7278	0.7392	0.5151	0.3406	0.1527	0.4951
Diff-Palm	200	1.0	0.549	0.118	0.069	0.111	0.8420	0.9111	0.8113	0.4237	0.6018	0.7180
Diff-Palm	500	1.0	0.766	0.108	0.068	0.112	0.8782	0.9601	0.9460	0.4643	0.6161	0.7729
Diff-Palm	800	1.0	0.922	0.072	0.069	0.112	0.8354	0.9014	0.8592	0.3369	0.5035	0.6873
PCE-Palm(Bézier)	–	–	0.402	0.171	0.099	0.116	0.6796	0.7740	0.6149	0.2972	0.4150	0.5561
PCE-Palm(poly)	–	1.0	0.351	0.186	0.041	0.110	0.8220	0.8687	0.7674	0.4373	0.5974	0.6986
Diff-Palm(Bézier)	500	–	0.629	0.198	0.171	0.114	0.6722	0.8236	0.7246	0.2732	0.3658	0.5719
Diff-Palm(poly)	500	1.0	0.766	0.108	0.068	0.112	0.8782	0.9601	0.9460	0.4643	0.6161	0.7729
Diff-Palm	500	0.25	0.748	0.121	0.107	0.113	0.8440	0.9134	0.8410	0.4162	0.5794	0.7188
Diff-Palm	500	0.5	0.764	0.118	0.088	0.117	0.8613	0.9230	0.8700	0.4268	0.5823	0.7327
Diff-Palm	500	1.0	0.766	0.108	0.068	0.112	0.8782	0.9601	0.9460	0.4643	0.6161	0.7729
Diff-Palm	500	2.0	0.784	0.102	0.070	0.109	0.8053	0.9308	0.9162	0.3697	0.4890	0.7022
Diff-Palm	500	4.0	0.780	0.103	0.095	0.108	0.7793	0.8804	0.8662	0.3041	0.4341	0.6528
Diff-Palm(first K)	500	1.0	0.475	0.043	0.117	0.11	0.7649	0.7571	0.5136	0.2502	0.0307	0.4633
Diff-Palm(last K)	500	1.0	0.766	0.108	0.068	0.112	0.8782	0.9601	0.9460	0.4643	0.6161	0.7729

Table 1. Verification performance of recognition models(ArcFace [7]) with the same hyperparameters used for various generated datasets, and without any fine-tuning on real data. Synthetic datasets default to be generated with $2k$ IDs and 20 samples per ID.

Methods	K	$C_{identity}$	D_{intra}	U_{class}	Perf.
Diff-Palm	0	0.5923	1.000	0.897	0.4951
Diff-Palm	200	0.9667	0.9615	0.980	0.7189
Diff-Palm	500	0.9981	0.9372	0.996	0.7729
Diff-Palm	800	0.9996	0.6659	0.999	0.6873
PCE-Palm(Bézier)	–	0.6046	1.1894	0.653	0.5561
PCE-Palm(poly)	–	0.6850	1.1816	0.958	0.6986
Diff-Palm(Bézier)	500	0.9952	0.9691	0.694	0.5719
Diff-Palm(poly)	500	0.9981	0.9372	0.996	0.7729

Table 2. Evaluation of synthetic datasets. $C_{identity}$, D_{intra} , and U_{class} represent identity consistency, intra-class diversity, and class uniqueness, respectively.

Comparing Palm Crease Representations We compare the performance of PCE-Palm [22] and our diffusion model by training them on different types of palm crease representations: Bézier creases [48] and polynomial creases, respectively. Each model is trained using consistent hyperparameters, with the only difference being the type of crease images used. As evidenced in Tab.1, the polynomial creases method significantly outperforms the Bézier creases. This result indicates that our polynomial crease representation more accurately bridges the gap between synthetic and real palmprints.

Evaluating Identity and Diversity Metrics We adopt identity consistency, intra-class diversity, and class uniqueness metrics from [24] to evaluate the respective properties of synthetic datasets. As shown in Tab.2, for our Diff-Palm, there exists a trade-off between identity consistency and intra-class diversity as parameter K is adjusted. For

$K = 500$, the generated dataset strikes a balance between them, leading to optimal recognition performance. When comparing generative methods with different palm crease representations, it is evident that the use of Bézier creases leads to a noticeable decline in class uniqueness, as opposed to polynomial creases. Our analyses indicate that the superior performance of our method is due to the *effective balance between identity consistency and intra-class diversity* achieved by the intra-class variation controllable method, as well as the *enhanced class uniqueness* resulting from the use of polynomial creases. In contrast, PCE-Palm suffers from low identity consistency and reduced class uniqueness, leading the poor performance. These analysis results are also validated by the t-SNE visualization, as shown in Fig.8. Further Details about these metrics are provided in the supplementary materials.

Effect of Palm Crease Similarity on Recognition We synthesize polynomial crease datasets with varying γ values to generate palmprint datasets through diffusion models. As shown in Tab.1, results indicate that recognition performance declines when γ is either greater than 1 or less than 1, corresponding to the expansion or contraction of the estimated distribution’s variance. We believe that when $\gamma > 1$, the generated data disrupts original distribution patterns, while when $\gamma < 1$, training recognition models becomes increasingly difficult. These results confirm the reasonableness and validity of our estimated distributions.

Comparing with Real Datasets and Other Methods We utilize seven public datasets to create a mixed dataset containing 2.2k IDs. The current SOTA palmprint gen-

Methods	Configs				Performance (TAR@FAR=1e-6) \uparrow					
	#IDs	# per ID	#Images	FT w/ Real	CASIA	PolyU	Tongji	MPD	XJTU-UP	Avg.
Real data	2.2k	–	29.3k	\times	0.9200	0.9196	0.9209	0.3877	0.6247	0.7546
IDiff-Face [2]	2k	20	40k	\times	0.7977	0.7720	0.6115	0.1847	0.2667	0.5265
Vec2Face [40]	2k	20	40k	\times	0.8201	0.8105	0.8199	0.2575	0.2578	0.5932
PCE-Palm [22]	2k	20	40k	\times	0.6796	0.7740	0.6149	0.2972	0.4150	0.5561
Diff-Palm	2k	20	40k	\times	0.8782	0.9601	0.9460	0.4643	0.6161	0.7729
PCE-Palm [22]	2k	20	40k	\checkmark	0.9415	0.9792	0.9393	0.6662	0.7948	0.8642
Diff-Palm	2k	20	40k	\checkmark	0.9787	0.9859	0.9744	0.5979	0.8433	0.8760
Diff-Palm	5k	20	100k	\times	0.8972	0.9757	0.9590	0.5048	0.7534	0.8180
Diff-Palm	10k	20	200k	\times	0.9072	0.9818	0.9632	0.5687	0.8143	0.8470
Diff-Palm	20k	20	400k	\times	0.9383	0.9795	0.9783	0.6304	0.8655	0.8784
Diff-Palm	30k	20	600k	\times	0.9472	0.9772	0.9772	0.6651	0.9015	0.8937
Diff-Palm	40k	20	800k	\times	0.9450	0.9799	0.9802	0.6641	0.9043	0.8947
Diff-Palm	50k	20	1M	\times	0.9542	0.9822	0.9848	0.6814	0.9032	0.9011
Diff-Palm	60k	20	1.2M	\times	0.9557	0.9865	0.9825	0.6856	0.9029	0.9026
Diff-Palm	2k	50	100k	\times	0.8810	0.9335	0.9185	0.4779	0.7214	0.7865
Diff-Palm	2k	100	200k	\times	0.9006	0.9436	0.9443	0.5522	0.7482	0.8178
Diff-Palm	2k	150	300k	\times	0.8817	0.9669	0.9482	0.5559	0.8043	0.8314
Diff-Palm	2k	200	400k	\times	0.9143	0.9710	0.9455	0.5775	0.8494	0.8515

Table 3. Verification performance of the recognition models across five public datasets, with the same hyperparameters used for both real and synthesized datasets. Diff-Palm is trained with $K = 500$ and $\gamma = 1.0$ by default.

eration method, PCE-Palm [22], and the face generation method [2, 40], are trained for comparison. By default, we train the recognition models on synthetic datasets without employing real data fine-tuning. As shown in Tab.3, the recognition model trained on the dataset generated by our method outperforms the models trained on real data across three public datasets, and achieves an average improvement. Furthermore, our approach significantly surpasses both PCE-Palm and facial models. We also conduct fine-tuning experiments using real data for a comprehensive comparison with PCE-Palm. More results are provided in the supplementary materials.

Impact of Synthesized Identity and Sample Quantity We generate datasets with varying numbers of identities, maintaining 20 samples per identity, to train recognition models. As evidenced in Tab.3, the performance of the recognition model steadily improves as the number of identities increases. The highest performance is observed when the number of identities reaches 60k. We also explore the impact of varying the number of samples per identity while keeping the number of identities constant. As shown in Tab.3, increasing the number of samples per identity from 20 to 200 results in continuous performance improvement. These findings demonstrate the scalability of our approach.

Ablation and Discussion of K -Step Noise-Sharing Sampling We generate palmprint datasets using two different noise-sharing strategies (i.e., applied during the first K

steps or the last K steps) and evaluate their performance. As shown in Tab.1, applying noise-sharing during the first K steps results in lower intra-class diversity in the generated datasets, leading to poorer recognition performance. Additionally, the K step noise-sharing sampling can serve as a plug-and-play method applicable to other diffusion-based generative models. We provide results applying this method to IDiff-Face [2] in the supplementary materials.

5. Conclusion

This paper proposes a polynomial-based palm crease representation, capable of generating a large-scale dataset with a distribution closely resembling that of real palm crease. Subsequently, an intra-class variation controllable diffusion model is introduced, with a simple yet effective K -step noise-sharing sampling, which enables the generation of palmprint datasets with adjustable intra-class variations. Experimental results indicate that our proposed method significantly reduces the gap between generated and real datasets. It is also the first time that the palmprint recognition model trained solely on our generated data, yet outperforms the model trained on real data.

Acknowledgments We would like to acknowledge Zhiyuan Wang and Yang Wu for their assistance in polynomial creases. This work is partly supported by the grants of the National Natural Science Foundation of China under Nos.62476077, 62076086, and 62272142.

References

- [1] Keivan Bahmani, Richard Plesh, Peter Johnson, Stephanie Schuckers, and Timothy Swyka. High fidelity fingerprint generation: Quality, uniqueness, and privacy. In *2021 IEEE International Conference on Image Processing (ICIP)*, pages 3018–3022. IEEE, 2021. 2
- [2] Fadi Boutros, Jonas Henry Grebe, Arjan Kuijper, and Naser Damer. Idiff-face: Synthetic-based face recognition through fuzzy identity-conditioned diffusion model. In *Proceedings of the IEEE/CVF International Conference on Computer Vision*, pages 19650–19661, 2023. 3, 8, 4
- [3] Hanqun Cao, Cheng Tan, Zhangyang Gao, Yilun Xu, Guangyong Chen, Pheng-Ann Heng, and Stan Z Li. A survey on generative diffusion models. *IEEE Transactions on Knowledge and Data Engineering*, 2024. 2
- [4] Sheng Chen, Yang Liu, Xiang Gao, and Zhen Han. Mobile-facenet: Efficient cnns for accurate real-time face verification on mobile devices. In *Chinese Conference on Biometric Recognition*, pages 428–438. Springer, 2018. 3
- [5] Florinel-Alin Croitoru, Vlad Hondru, Radu Tudor Ionescu, and Mubarak Shah. Diffusion models in vision: A survey. *IEEE Transactions on Pattern Analysis and Machine Intelligence*, 45(9):10850–10869, 2023. 2, 4
- [6] Ekin D Cubuk, Barret Zoph, Jonathon Shlens, and Quoc V Le. Randaugment: Practical automated data augmentation with a reduced search space. In *Proceedings of the IEEE/CVF conference on computer vision and pattern recognition workshops*, pages 702–703, 2020. 6
- [7] Jiankang Deng, Jia Guo, Niannan Xue, and Stefanos Zafeiriou. Arcface: Additive angular margin loss for deep face recognition. In *CVPR*, pages 4690–4699, 2019. 3, 6, 7
- [8] Yu Deng, Jiaolong Yang, Dong Chen, Fang Wen, and Xin Tong. Disentangled and controllable face image generation via 3d imitative-contrastive learning. In *IEEE Computer Vision and Pattern Recognition*, 2020. 2
- [9] Prafulla Dhariwal and Alexander Nichol. Diffusion models beat gans on image synthesis. *Advances in neural information processing systems*, 34:8780–8794, 2021. 5
- [10] Alexey Dosovitskiy, Lucas Beyer, Alexander Kolesnikov, Dirk Weissenborn, Xiaohua Zhai, Thomas Unterthiner, Mostafa Dehghani, Matthias Minderer, Georg Heigold, Sylvain Gelly, Jakob Uszkoreit, and Neil Houlsby. An image is worth 16x16 words: Transformers for image recognition at scale. *ArXiv*, abs/2010.11929, 2020. 3
- [11] Joshua J Engelsma, Steven A Grosz, and Anil K Jain. Prints-gan: Synthetic fingerprint generator. *IEEE Transactions on Pattern Analysis and Machine Intelligence*, 2022. 2
- [12] Dandan Fan, Xu Liang, Wei Jia, Junan Chen, and David Zhang. A novel hybrid fusion combining palmprint and palm vein for large-scale palm-based recognition. *IEEE Transactions on Systems, Man, and Cybernetics: Systems*, 2024. 3
- [13] Lunke Fei, Guangming Lu, Wei Jia, Shaohua Teng, and David Zhang. Feature extraction methods for palmprint recognition: A survey and evaluation. *IEEE Transactions on Systems, Man, and Cybernetics: Systems*, 49(2):346–363, 2018. 1
- [14] Chaoyou Fu, Xiang Wu, Yibo Hu, Huaibo Huang, and Ran He. Dual variational generation for low shot heterogeneous face recognition. *Advances in neural information processing systems*, 32, 2019. 2
- [15] Chaoyou Fu, Xiang Wu, Yibo Hu, Huaibo Huang, and Ran He. Dvg-face: Dual variational generation for heterogeneous face recognition. *IEEE transactions on pattern analysis and machine intelligence*, 44(6):2938–2952, 2021. 2
- [16] Angelo Genovese, Vincenzo Piuri, Konstantinos N Plataniotis, and Fabio Scotti. Palmnet: Gabor-pca convolutional networks for touchless palmprint recognition. *IEEE TIFS*, 14(12):3160–3174, 2019. 3
- [17] Ian Goodfellow, Jean Pouget-Abadie, Mehdi Mirza, Bing Xu, David Warde-Farley, Sherjil Ozair, Aaron Courville, and Yoshua Bengio. Generative adversarial networks. *Communications of the ACM*, 63(11):139–144, 2020. 1
- [18] Steven A Grosz and Anil K Jain. Genpalm: Contactless palmprint generation with diffusion models. *arXiv preprint arXiv:2406.00287*, 2024. 4
- [19] Kaiming He, Xiangyu Zhang, Shaoqing Ren, and Jian Sun. Deep residual learning for image recognition. In *CVPR*, pages 770–778, 2016. 6
- [20] Jonathan Ho, Ajay Jain, and Pieter Abbeel. Denoising diffusion probabilistic models. *Advances in neural information processing systems*, 33:6840–6851, 2020. 1, 2
- [21] Wei Jia, Qiang Ren, Yang Zhao, Shujie Li, Hai Min, and Yanxiang Chen. Eepnet: An efficient and effective convolutional neural network for palmprint recognition. *Pattern Recognition Letters*, 159:140–149, 2022. 3
- [22] Jianlong Jin, Lei Shen, Ruixin Zhang, Chenglong Zhao, Ge Jin, Jingyun Zhang, Shouhong Ding, Yang Zhao, and Wei Jia. Pce-palm: Palm crease energy based two-stage realistic pseudo-palmprint generation. In *Proceedings of the AAAI Conference on Artificial Intelligence*, pages 2616–2624, 2024. 1, 2, 3, 4, 5, 7, 8
- [23] Indu Joshi, Marcel Grimmer, Christian Rathgeb, Christoph Busch, Francois Bremond, and Antitza Dantcheva. Synthetic data in human analysis: A survey. *IEEE Transactions on Pattern Analysis and Machine Intelligence*, 2024. 1
- [24] Minchul Kim, Feng Liu, Anil Jain, and Xiaoming Liu. Dc-face: Synthetic face generation with dual condition diffusion model. In *Proceedings of the IEEE/CVF conference on computer vision and pattern recognition*, pages 12715–12725, 2023. 2, 7
- [25] Subhadeep Koley, Ayan Kumar Bhunia, Deeptanshu Sekhri, Aneeshan Sain, Pinaki Nath Chowdhury, Tao Xiang, and Yi-Zhe Song. It’s All About Your Sketch: Democratising Sketch Control in Diffusion Models. In *CVPR*, 2024. 2
- [26] Ajay Kumar. Incorporating cohort information for reliable palmprint authentication. In *2008 Sixth Indian conference on computer vision, graphics & image processing*, pages 583–590. IEEE, 2008. 5, 1
- [27] Ilya Loshchilov and Frank Hutter. Decoupled weight decay regularization. *arXiv preprint arXiv:1711.05101*, 2017. 6
- [28] Camillo Lugaresi, Jiuqiang Tang, Hadon Nash, Chris McClanahan, Esha Uboweja, Michael Hays, Fan Zhang, Chuoling Chang, Ming Guang Yong, Juhyun Lee, Wan-Teh

- Chang, Wei Hua, Manfred Georg, and Matthias Grundmann. Mediapipe: A framework for building perception pipelines, 2019. [1](#)
- [29] Wojciech Michal Matkowski, Tingting Chai, and Adams Wai Kin Kong. Palmprint recognition in uncontrolled and uncooperative environment. *IEEE TIFS*, 2019. [5](#), [1](#)
- [30] Chong Mou, Xintao Wang, Liangbin Xie, Yanze Wu, Jian Zhang, Zhongang Qi, and Ying Shan. T2i-adapter: Learning adapters to dig out more controllable ability for text-to-image diffusion models. In *Proceedings of the AAAI Conference on Artificial Intelligence*, pages 4296–4304, 2024. [2](#)
- [31] Thu Nguyen-Phuoc, Chuan Li, Lucas Theis, Christian Richardt, and Yong-Liang Yang. Hologan: Unsupervised learning of 3d representations from natural images. In *Proceedings of the IEEE/CVF International Conference on Computer Vision*, pages 7588–7597, 2019. [2](#)
- [32] Haibo Qiu, Baosheng Yu, Dihong Gong, Zhifeng Li, Wei Liu, and Dacheng Tao. Synface: Face recognition with synthetic data. In *Proceedings of the IEEE/CVF International Conference on Computer Vision*, pages 10880–10890, 2021. [2](#)
- [33] Robin Rombach, Andreas Blattmann, Dominik Lorenz, Patrick Esser, and Björn Ommer. High-resolution image synthesis with latent diffusion models. In *Proceedings of the IEEE/CVF conference on computer vision and pattern recognition*, pages 10684–10695, 2022. [2](#)
- [34] Chitwan Saharia, William Chan, Huiwen Chang, Chris Lee, Jonathan Ho, Tim Salimans, David Fleet, and Mohammad Norouzi. Palette: Image-to-image diffusion models. In *ACM SIGGRAPH 2022 conference proceedings*, pages 1–10, 2022. [2](#)
- [35] Huikai Shao, Dexing Zhong, and Xuefeng Du. Effective deep ensemble hashing for open-set palmprint recognition. *Journal of Electronic Imaging*, 29(1):013018, 2020. [5](#), [1](#)
- [36] Lei Shen, Jianlong Jin, Ruixin Zhang, Huaen Li, Kai Zhao, Yingyi Zhang, Jingyun Zhang, Shouhong Ding, Yang Zhao, and Wei Jia. Rpg-palm: Realistic pseudo-data generation for palmprint recognition. In *Proceedings of the IEEE/CVF International Conference on Computer Vision*, pages 19605–19616, 2023. [1](#), [2](#), [3](#)
- [37] Alon Shoshan, Nadav Bhonker, Emanuel Ben Baruch, Ori Nizan, Igor Kviatkovsky, Joshua Engelsma, Manoj Aggarwal, and Gérard Medioni. Fpgan-control: A controllable fingerprint generator for training with synthetic data. In *Proceedings of the IEEE/CVF Winter Conference on Applications of Computer Vision*, pages 6067–6076, 2024. [2](#)
- [38] Zhenan Sun, Tieniu Tan, Yunhong Wang, and Stan Z Li. Ordinal palmprint representation for personal identification [representation read representation]. In *CVPR*, pages 279–284. IEEE, 2005. [5](#), [1](#)
- [39] Hao Wang, Yitong Wang, Zheng Zhou, Xing Ji, Dihong Gong, Jingchao Zhou, Zhifeng Li, and Wei Liu. Cosface: Large margin cosine loss for deep face recognition. In *CVPR*, pages 5265–5274, 2018. [3](#)
- [40] Haiyu Wu, Jaskirat Singh, Sicong Tian, Liang Zheng, and Kevin W. Bowyer. Vec2face: Scaling face dataset generation with loosely constrained vectors. *ICLR*, 2025. [8](#), [3](#)
- [41] Yichao Yan, Zanwei Zhou, Zi Wang, Jingnan Gao, and Xiaokang Yang. Dialoguenerf: towards realistic avatar face-to-face conversation video generation. *Visual Intelligence*, 2: 24, 2024. [2](#)
- [42] Ziyuan Yang, Huijie Huangfu, Lu Leng, Bob Zhang, Andrew Beng Jin Teoh, and Yi Zhang. Comprehensive competition mechanism in palmprint recognition. *IEEE Transactions on Information Forensics and Security*, 18:5160–5170, 2023. [3](#)
- [43] Ziyuan Yang, Wenjun Xia, Yifan Qiao, Zexin Lu, Bob Zhang, Lu Leng, and Yi Zhang. Co3net: Coordinate-aware contrastive competitive neural network for palmprint recognition. *IEEE Transactions on Instrumentation and Measurement*, 2023. [3](#)
- [44] David Zhang, Wai-Kin Kong, Jane You, and Michael Wong. Online palmprint identification. *IEEE Transactions on pattern analysis and machine intelligence*, 25(9):1041–1050, 2003. [5](#), [1](#)
- [45] Lin Zhang, Lida Li, Anqi Yang, Ying Shen, and Meng Yang. Towards contactless palmprint recognition: A novel device, a new benchmark, and a collaborative representation based identification approach. *Pattern Recognition*, 69:199–212, 2017. [5](#), [1](#)
- [46] Yingyi Zhang, Lin Zhang, Xiao Liu, Shengjie Zhao, Ying Shen, and Yukai Yang. Pay by showing your palm: A study of palmprint verification on mobile platforms. In *2019 IEEE International Conference on Multimedia and Expo (ICME)*, pages 862–867, 2019. [1](#)
- [47] Yingyi Zhang, Lin Zhang, Ruixin Zhang, Shaoxin Li, Jilin Li, and Feiyue Huang. Towards palmprint verification on smartphones. *arXiv preprint arXiv:2003.13266*, 2020. [5](#), [1](#)
- [48] Kai Zhao, Lei Shen, Yingyi Zhang, Chuhan Zhou, Tao Wang, Ruixin Zhang, Shouhong Ding, Wei Jia, and Wei Shen. Bézierpalm: A free lunch for palmprint recognition. In *European Conference on Computer Vision*, pages 19–36. Springer, 2022. [1](#), [2](#), [3](#), [7](#)
- [49] Tianpeng Zheng, Yanxiang Chen, Xinzhe Wen, Yancheng Li, and Zhiyuan Wang. Research on diffusion model generated video datasets and detection benchmarks. *Journal of Image and Graphics*, 2024. [2](#)
- [50] Dexing Zhong and Jinsong Zhu. Centralized large margin cosine loss for open-set deep palmprint recognition. *IEEE TCSVT*, 2019. [3](#)

Diff-Palm: Realistic Palmprint Generation with Polynomial Creases and Intra-Class Variation Controllable Diffusion Models

Supplementary Material

This supplementary materials provide the following contents:

- an overview of datasets used: both public datasets and anonymous datasets.
- evaluation metrics.
- additional experimental results.
- discussions on proposed sampling methods and validation approaches.

6. Datasets

6.1. Public Datasets

We utilize seven publicly available palmprint datasets, including, CASIA [38], PolyU [44], Tongji [45], MPD [47], XJTU-UP [35], IITD [26], and NTU-CP-v1 [29], with detailed information provided in Tab.4 and example images shown in Fig.9. Following the open-set protocol, we divide the first five palmprint datasets into training and testing sets in a 1:1 ratio based on the number of IDs, ensuring no overlap between the IDs in the training and testing sets. Due to the limited number of images in the other two datasets, we used them exclusively for training.

6.2. Collected Anonymous Dataset

We employ keywords such as "hand," "palm," and "palm print" to search for images on the Internet. After obtaining these images, we utilize Mediapipe [28] to detect the presence and completeness of palms in the images. Following this filtering process, we apply the detect-then-crop protocol in [46] to extract the Region of Interest (ROI) of the palmprints. We have acquired 48,000 complete palmprint ROI images, which are then used to train our generative model. Example images are shown in Fig.10. Due to relevant privacy protection regulations, we will release the URLs to these images.

Datasets	#ID	#Images	Devices
CASIA	620	5502	Digital camera
PolyU	388	7738	Scanner
Tongji	600	12,000	Digital camera
MPD	400	16,000	Mobile phone
XJTU-UP	200	7900	Mobile phone
IITD	460	2601	Digital camera
NTU-CP-v1	652	2390	Digital camera

Table 4. Details of the seven public palmprint datasets.

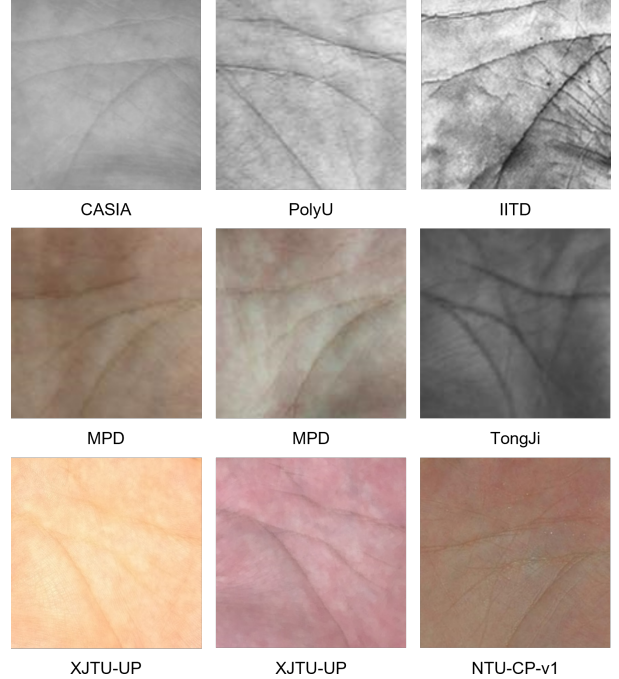


Figure 9. Example images of public palmprint datasets.



Figure 10. Example images of collected anonymous datasets.

7. Evaluation Metrics

7.1. Performance Metrics

we adopt the TAR(True accept ratio)@FAR(False accept ratio) metric, which is a widely used metric in open-set recognition tasks. It quantifies the system’s ability to correctly ac-

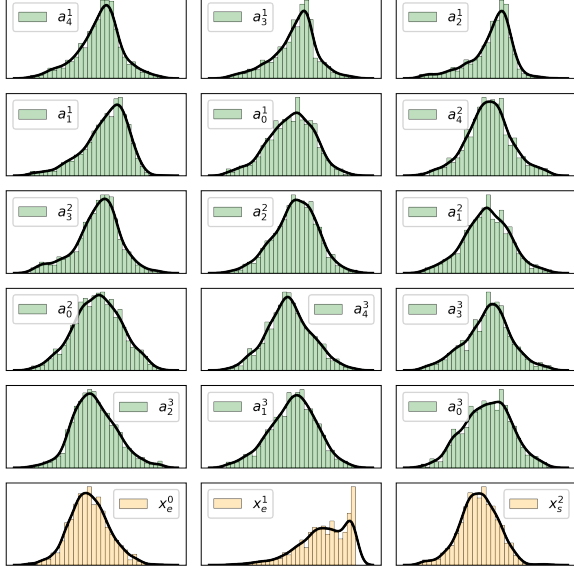


Figure 11. Histograms of the 15 polynomial coefficients and the x-coordinates for 3 endpoints

cept genuine instances while controlling the rate of falsely accepted impostors. To compute TAR@FAR, one first determines the threshold t under the specific FAR, which represents the proportion of non-genuine instances incorrectly accepted as genuine. At this threshold t , the TAR is calculated as the proportion of genuine instances correctly accepted, as follows,

$$\text{TAR}(t) = \frac{\text{Number of True Acceptances}}{\text{Total Number of Genuine Attempts}}.$$

7.2. Datasets Evaluation Metrics

We utilize three metrics derived from [24] to evaluate the synthesized dataset. Specifically, we employ a recognition model F_{eval} , pre-trained on a real dataset to extract features from each image in the dataset. For the image X_i^c , i -th sample within c -th label, we denote its feature as $f_i^c = F_{eval}(X_i^c)$. We use cosine similarity to measure the distance between two samples. Additionally, we denote the feature of the center of each class as \bar{f}^c for $c \in \{1, \dots, C\}$, which is also the spherical mean of the samples within the same label.

Class Uniqueness. We first define U_c as follows,

$$U_c = \{\bar{f}^c : d(\bar{f}^c, \bar{f}^m) > r, m < n, n, m \in \{1, \dots, C\}\},$$

where $d(\cdot, \cdot)$ is the cosine distance. The U_c is the set of unique subjects determined by the threshold r . For this metric, we define $U_{class} := |U_c| / C$, the ratio between the number of unique subjects and the number of total labels.

Identity Consistency. To measure how consistent the synthesized samples are in adhering to the label condition, we define $C_{identity}$ as

$$C_{identity} = \frac{1}{C} \sum_{c=1}^C \frac{1}{N_c} \sum_{i=1}^{N_c} d(f_i^c, \bar{f}^c) < r,$$

which is the ratio of individual features f_i^c being close to the class center \bar{f}^c . For a given threshold r , higher values of $C_{identity}$ mean the samples under the same label are more likely to be the same subject.

Intra-class Diversity. We aim to measure how diverse the generated samples are under the same label condition, as well as the diversity is in the style of an image, not in the subject's identity. In the original paper [24], the Inception Network pre-trained on ImageNet is utilized to extract the style information of the images. However, since palmprints are significantly different from the images in ImageNet, and are often simple and relatively uniform, we employ a pixel-based diversity measure. Specifically, we adopt $\bar{X}^c = \frac{1}{N_c} \sum_{i=0}^{N_c} X_i^c$ denotes the mean image of c class, and diversity is defined as:

$$D_{intra} = \frac{1}{C} \sum_{c=1}^C \frac{1}{N_c} \sum_{i=1}^{N_c} \|X_i^c - \bar{X}^c\|_1,$$

where $\|\cdot\|_1$ denotes $L1$ norm. We take the D_{intra} value of datasets generated by Diff-Palm with $K = 0$ as the baseline, normalizing it to 1.0, and adjusting all other values accordingly.

8. Additional Experimental Results

8.1. Histogram of Polynomial Coefficients

We use three polynomial curves to mark the three main lines of the palmprint. Each polynomial curve contains five coefficients. Therefore, we plot the histograms for all 15 coefficients, as shown in Fig. 11. Additionally, we conduct a statistical analysis of the x-coordinates for the endpoints of 3 palm lines.

8.2. Performance on Individual Public Datasets

We conduct recognition experiments on individual public datasets. The experimental results are presented in the first section of Tab. 5. The performance achieved on individual public datasets is significantly lower compared to that on mixed public datasets.

8.3. Further Fine-Tuning Experiments

We adopt Diff-Palm to generate datasets with a large number of IDs. These datasets are used to pre-train the recognition model, which is subsequently fine-tuned using real datasets. As shown in the second section of Tab. 5, the performance of our method consistently improves after fine-tuning.

Methods	Configs			Performance (TAR@FAR=1e-6) \uparrow					
	#IDs	#Images	FT w/ Real	CASIA	PolyU	TongJi	MPD	XJTU-UP	Avg.
CASIA	310	2510	\times	0.7243	0.7198	0.5952	0.0964	0.1963	0.4664
PolyU	194	3869	\times	0.5235	0.7574	0.4322	0.0746	0.1402	0.3856
TongJi	300	6000	\times	0.7344	0.7115	0.8032	0.1476	0.0977	0.4989
MPD	200	8000	\times	0.8839	0.8254	0.8599	0.3745	0.2939	0.6455
XJTU-UP	100	3950	\times	0.7741	0.7518	0.7183	0.1805	0.4549	0.5759
IITD	460	2601	\times	0.3895	0.5205	0.1024	0.0397	0.0681	0.2240
NTU-CP-v1	652	2390	\times	0.6652	0.8330	0.7970	0.1628	0.2588	0.5434
Diff-Palm	5k	100k	\checkmark	0.9783	0.9850	0.9848	0.6754	0.8966	0.9040
Diff-Palm	10k	200k	\checkmark	0.9857	0.9910	0.9905	0.7400	0.9442	0.9303
Diff-Palm	20k	400k	\checkmark	0.9832	0.9943	0.9920	0.7922	0.9484	0.9420
Diff-Palm	30k	600k	\checkmark	0.9870	0.9945	0.9941	0.8044	0.9570	0.9474
Diff-Palm	40k	800k	\checkmark	0.9827	0.9949	0.9936	0.8179	0.9593	0.9497
Diff-Palm	50k	1M	\checkmark	0.9843	0.9965	0.9933	0.8498	0.9700	0.9588
Diff-Palm(10k)	2k	40k	\times	0.8598	0.9472	0.9113	0.4124	0.6133	0.7488
Diff-Palm(48k)	2k	40k	\times	0.8782	0.9601	0.9460	0.4643	0.6161	0.7729
Real data(R50)	2.2k	29.3k	\times	0.9429	0.8927	0.9449	0.3974	0.6111	0.7577
IDiff-Face(R50) [2]	2k	40k	\times	0.7944	0.7404	0.6208	0.1793	0.2734	0.5217
PCE-Palm(R50) [22]	2k	40k	\times	0.5749	0.7188	0.5835	0.2738	0.4347	0.5171
Diff-Palm(R50)	2k	40k	\times	0.8708	0.9558	0.9577	0.4472	0.6266	0.7716
Real data(MBF)	2.2k	29.3k	\times	0.9323	0.9071	0.9247	0.3616	0.6067	0.7466
IDiff-Face(MBF) [2]	2k	40k	\times	0.7732	0.7445	0.6507	0.1667	0.2259	0.5120
PCE-Palm(MBF) [22]	2k	40k	\times	0.6112	0.7379	0.5266	0.2695	0.4013	0.5093
Diff-Palm(MBF)	2k	40k	\times	0.8546	0.9489	0.9409	0.4297	0.6177	0.7584
Real data(ViT)	2.2k	29.3k	\times	0.8279	0.6909	0.7390	0.2132	0.2826	0.5505
IDiff-Face(ViT) [2]	2k	40k	\times	0.6676	0.5968	0.5304	0.1234	0.1783	0.4193
Vec2Face(ViT) [40]	2k	40k	\times	0.6967	0.5075	0.4406	0.0962	0.1108	0.3704
PCE-Palm(ViT) [22]	2k	40k	\times	0.6012	0.4918	0.4604	0.1303	0.1515	0.3670
Diff-Palm(ViT)	0.6814	0.7920	0.7792	0.2798	0.3754	0.5816			

Table 5. Comparison performance of recognition models trained on various datasets. Results are reported in TAR@FAR=1e-6. ‘R50’, ‘MBF’ and ‘ViT’ represent ResNet-50[7], MobileFaceNet[4] and ViT-t [10], respectively

8.4. Polynomial Creases Similarity Control

We generate a polynomial creases dataset and control the overall similarity using different γ . As illustrated in Fig. 12, we can observe that when γ is less than 1.0, the similarity of the generated polynomial creases increases. Conversely, when γ is greater than 1.0, the overall similarity decreases, and the generated creases become more random.

8.5. Additional Ablation Experiments

Smaller Anonymous Datasets We have collected an anonymous dataset containing 48,000 images, which we used to train the generative model. We also experiment with training Diff-Palm using a smaller dataset of 10,000 images. The experimental results are presented in the third section of Tab. 5. We observe that the performance of Diff-Palm

trained with 10,000 images is inferior to that trained with 48,000 images. However, it still achieves results comparable to those obtained with real datasets.

Different Recognition Backbone We conduct comparative experiments using different recognition backbones (modified Resnet-50 [7], MobileFaceNet [4] and ViT-t [10]). The experimental results are shown in the last three sections of Tab. 5. We arrive at the same conclusions as those in the main paper.

9. More Discussion

9.1. K-Step Noise-Sharing Sampling

To verify that K -step noise-sharing sampling can be applied to other diffusion-based methods, we use the offi-

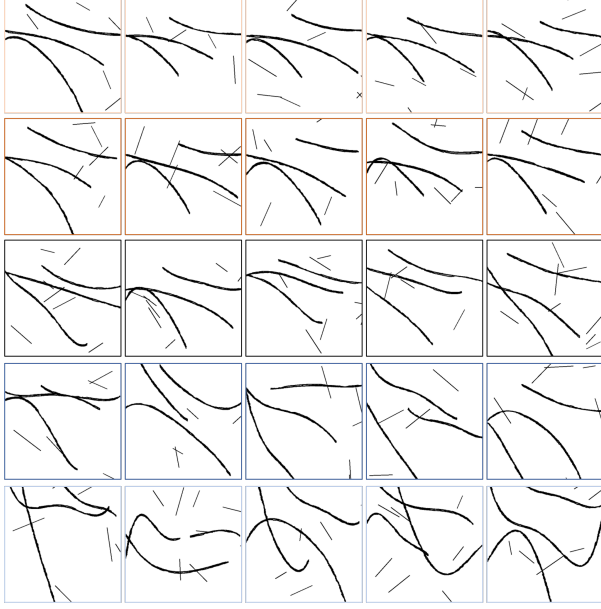


Figure 12. Synthesized polynomial crease images with varying γ . From top to bottom, the γ is set to 0.25, 0.5, 1.0, 2.0, and 4.0, respectively



Figure 13. Synthesized face images by IDiff-Face[2], (a) with noise-sharing in first 500 sampling steps, (b) with noise-sharing in last 500 sampling steps, (c) without noise-sharing, as well as cosine similarity calculated between adjacent face images

cially released pre-trained IDiff-Face model [2] and apply our K -step noise-sharing sampling to obtain facial images, as shown in Fig.13. We set $K = 500$ with a total step of $T = 1000$. Each row of images is generated from the same ID condition. Moreover, we employ a pre-trained fa-

cial recognition model to extract features from each image and calculate the cosine similarity between adjacent face images. It is evident that applying K -step noise-sharing sampling significantly enhances the identity consistency of the generated results. Additionally, applying noise-sharing in the last K steps further improves the identity consistency of the generated outcomes.

9.2. Validation Set

In PCE-Palm, they first split several public datasets into training and testing sets in a 1:1 ratio and then mixed all the testing sets from the public datasets for evaluation with the trained recognition model. However, due to different collection devices, environments, etc., the various public datasets have significant style differences. When the recognition model is tested on the mixed testing set, it is easy to distinguish an identity from one dataset from identities in other datasets. In contrast, we adopt a more general validation approach. After splitting the public data into training and testing sets in a 1:1 ratio, we validate each dataset separately. Subsequently, we average the validation results from each dataset.